Inorganic Chemistry

Article

pubs.acs.org/IC

Tetrathiafulvalene-1,3,5-triazines as (Multi)Donor–Acceptor Systems with Tunable Charge Transfer: Structural, Photophysical, and Theoretical Investigations

Flavia Pop,[†] François Riobé,[†] Sabine Seifert,[†] Thomas Cauchy,[†] Jie Ding,[‡] Nathalie Dupont,[‡] Andreas Hauser,*[,‡] Marius Koch,[‡] and Narcis Avarvari*[,†]

[†]LUNAM Université, Université d'Angers, CNRS UMR 6200, Laboratoire MOLTECH Anjou, 2 bd Lavoisier, 49045 Angers Cedex, France

[‡]Department of Physical Chemistry, University of Geneva, 30 Quai Ernest Ansermet, 1211 Geneva, Switzerland

Supporting Information

ABSTRACT: Palladium-catalyzed cross-coupling reactions between chlorinated 1,3,5-triazines (TZ) and tetrathiafulvalene (TTF) trimethyltin derivatives afford mono- and C_3 symmetric tris(TTF)-triazines as donor–acceptor compounds in which the intramolecular charge transfer (ICT) is modulated by the substitution scheme on TTF and TZ and by chemical or electrochemical oxidation. The TTF-TZ-Cl_2 and $(SMe)_2$TTF-TZ-Cl_2 derivatives show fully planar structures in the solid state as a consequence of the conjugation between the two units. Electrochemical and photophysical investigations, supported by theoretical calculations, clearly demonstrate that the lowest excited state can be ascribed to the intramolecular charge transfer (ICT) π(TTF)→π^*(TZ) transition. The tris(TTF) compound $[(SMe)_2TTF]_3$-TZ shows fluorescence when excited in the ICT band, and the emission is quenched upon oxidation. The radical cations $TTF^{+\bullet}$ are easily observed in all of the cases through chemical and electrochemical oxidation by steady-state absorption experiments. In the case of $[(SMe)_2TTF]_3$-TZ, a low energy band at 5000 cm^{-1}, corresponding to a coupling between $TTF^{+\bullet}$ and TTF units, is observed. A crystalline radical cation salt with the TTF-TZ-Cl_2 donor and PF_6^- anion, prepared by electrocrystallization, is described.

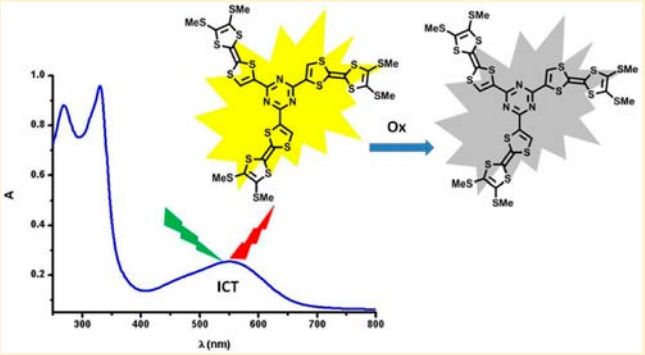

INTRODUCTION

Donor–acceptor (D–A) systems with intramolecular charge transfer (ICT) states proved their potential for organic optical and electronic functional materials with low energy-gaps.[1] Very useful and versatile π electron donor units are the tetrathiafulvalene (TTF) derivatives, extensively investigated in various fields,[2] which can be reversibly oxidized to the stable radical cation $TTF^{+\bullet}$ and dication TTF^{2+} at relative low potentials or by the use of chemical oxidants. These oxidized species, together with the neutral form, show distinct features in their absorption spectra.[3] It is thus not surprising that the TTF unit has been associated with diverse electron acceptors in D–A dyads with potential interest in the fields of photovoltaics, nonlinear optics, and molecular (opto)electronics.[4] In recent years, much effort has been devoted to the synthesis and physicochemical investigations of diverse TTF–acceptor systems, in which various linkers, in particular fused aromatics,[5] between the donor and acceptor units have been employed as a means to control and tune the ICT bands. In these fused D–A compounds, the conjugated bridges ensure efficient through bond ICT. Derivatives in which the ICT band has also a through bond nature, despite the less efficient conjugation between the moieties, are those with the TTF unit directly connected to the acceptor through a σ bond. However, comparatively, such systems are less numerous and include, for example, TTF-benzothiadiazole,[6] TTF-pyridinium,[7] or TTF-oxophenalenoxyl[8] derivatives. Some of us have recently described TTF-1,3,5-triazine (TTF-TZ) D–A compounds (**1** and **2** in Chart 1), in which π(TTF)→π^*(TZ) ICT bands have been experimentally and theoretically characterized,[9] and also TTF-triazine-dipicolylamine ligands, where the TTF-triazine moiety was used as a platform for the attachment of dipicolylamine (dpa) groups,[10] to access redox active ligands.[11] The interest in the use of the 1,3,5-triazine (TZ) ring, besides the electron poor character, relies upon its sequential functionalization up to C_3 symmetric derivatives starting from the commercially available trichlorotriazine,[12] and also upon the use as active component in optoelectronic materials.[13] Note that, apart the parent (tris)TTF-TZ compound **4a** (Chart 1) previously isolated in traces,[9] only one other C_3 symmetric tris(TTF)-triazine derivative has been described, yet with a

Received: December 12, 2012
Published: April 5, 2013

   dx.doi.org/10.1021/ic3027336 | *Inorg. Chem.* 2013, 52, 5023–5034

Chart 1

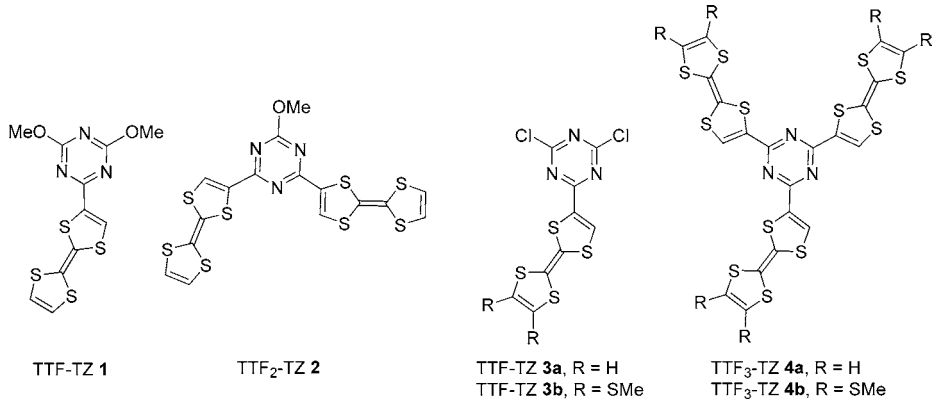

Scheme 1. Synthetic Routes for the TTF_n-TZ (n = 1−3) 1−4

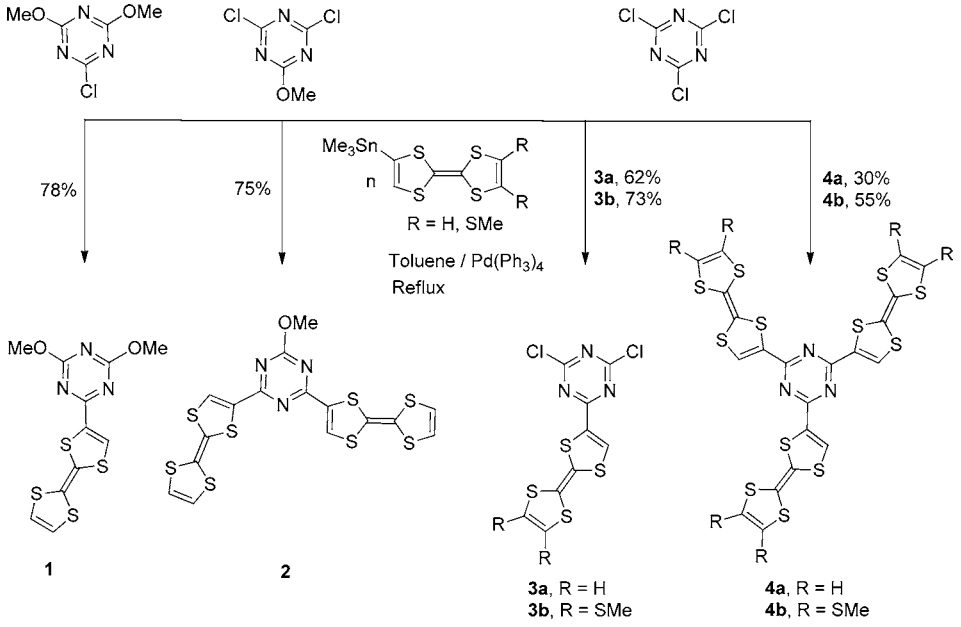

longer conjugated linker between the TZ and TTF units.[14] The interest in such multi(TTF) systems, additionally provided with ICT, relies on the possibility of accessing sequentially mixed valence states with optimized absorption properties in the visible and near IR, and hence a possible modulation of the photophysical properties. Moreover, variation of the substitution scheme on the triazine ring allows for a fine-tuning of its electron accepting properties, which influences the energy of the ICT band.

This article deals with the synthesis, spectroscopic, and photophysical study of the D−A compounds **1**−**4**, together with the structural characterization of the derivatives TTF-TZ **3**. Theoretical calculations at the DFT and TDDFT levels support the D−A nature of the TTF_n-TZ (n = 1−3) compounds and help in the understanding of the absorption properties and especially at the characterization of the ICT bands. A radical cation salt of the donor **3a** is also described.

RESULTS AND DISCUSSION

Synthesis and Solid-State Structures of 3a and 3b. In the previous work, the methoxy derivatives **1** and **2** were synthesized by the direct nucleophilic substitution between lithiated TTF and TZ-Cl_3, followed by quenching with MeONa, or lithiated TTF and the corresponding methoxychlorotriazine precursors.[9] However, the reported yields for both compounds were rather low (11% for **1** and 21% for **2**), and, moreover, the tris(TTF) compound **4a** was isolated only in traces and characterized by mass spectrometry. We have therefore decided to develop a more efficient strategy for the synthesis of TTF-TZ compounds. When the precursors $(OMe)_2$-TZ-Cl and (OMe)-TZ-Cl_2 were reacted with the tin derivative TTF-$SnMe_3$[15] under palladium-catalyzed Stille cross-coupling conditions, the D−A compounds **1** and **2** were isolated in 78% and 75% yields, respectively, after chromatographic workup (Scheme 1). Thus, the cross-coupling strategy is much more adapted than the nucleophilic substitution for the attachment of TTF units to the triazine ring, and it was therefore applied for the preparation of the new compounds **3** and **4**. The C_3 symmetric tris(TTF) **4a** was now obtained in 30% yield, and, despite its lack of solubility, it was characterized, besides MS, by ^{1}H NMR and elemental analysis. The more soluble tris(TTF) derivative **4b** was prepared by reacting the precursor $(MeS)_2$TTF-$SnMe_3$[16] in the same conditions. Moreover, to tune the ICT band by the substitution scheme on the triazine ring, the (mono)TTF dichloro-triazines **3a**,**b** have been prepared and isolated in good yields. All of the

dx.doi.org/10.1021/ic3027336 | Inorg. Chem. 2013, 52, 5023−5034

compounds have been obtained as red (**1**), dark purple (**2**), or black (**3**,**4**) solids. Unfortunately, this strategy did not allow the preparation of TTF_2-TZ-Cl derivatives regardless of the stoichiometry employed, very likely because they are more reactive toward the cross-coupling than Cl_3-TZ or TTF-TZ-Cl_2 **3a**,**b**.

Suitable single crystals for X-ray analysis have been grown for **3a**,**b** upon slow evaporation of solutions in dichloromethane (DCM) and cyclohexane. TTF-TZ-Cl_2 **3a** crystallizes as dark blue plates in the monoclinic system, space group $P2_1/c$, with one independent molecule in the unit cell. The donor TTF and acceptor TZ units are coplanar, as indicated by the dihedral angle TTF···TZ of 0.4° (Figure 1), a likely consequence of the conjugation between them. This feature has been also noticed in the case of the $(OMe)_2$-TZ-TTF derivative.[9]

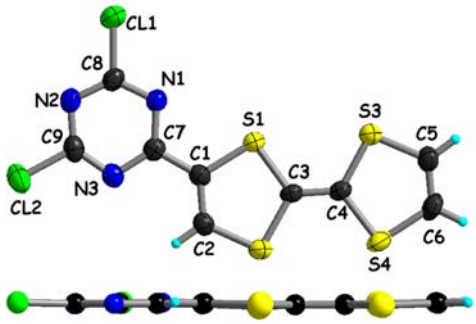

Figure 1. Molecular structure of **3a** with numbering scheme (top, ellipsoids at 50%), and a side view of the molecule (bottom).

The bond lengths (Table 1) are typical for neutral TTF units, as indicated by the value of the C3═C4 bond of

Table 1. Selected Bond Distances for 3a, 3b, and [(3a)(PF_6)]

bond length (Å)					
3a		**3b**		[(**3a**)(PF_6)]	
C3−C4	1.344(4)	C3−C4	1.352(6)	C3−C4	1.384(8)
S4−C4	1.763(3)	S3−C4	1.758(4)	S4−C4	1.721(5)
S3−C4	1.756(3)	S4−C4	1.755(4)	S3−C4	1.728(6)
S2−C2	1.717(3)	S2−C2	1.719(5)	S2−C2	1.713(7)
S2−C3	1.768(3)	S2−C3	1.763(5)	S2−C3	1.722(6)
S1−C3	1.758(3)	S1−C3	1.759(5)	S1−C3	1.725(5)
C1−C7	1.444(4)	C1−C9	1.441(6)	C6−C7	1.471(7)
C9−Cl2	1.732(3)	C10−Cl1	1.727(5)	C9−Cl2	1.713(6)
C8−Cl1	1.724(3)	C11−Cl2	1.721(5)	C8−Cl1	1.702(6)

1.344(4) Å and the average of the internal S−C bonds amounting to 1.761 Å. Compound **3b** crystallizes as violet plates in the monoclinic system, space group $P2_1/c$, with one independent molecule in the unit cell. Once again, the TZ and TTF units are coplanar, with the corresponding dihedral angle measuring 0.9°, excepting the methyl groups pointing in opposite directions to the TTF mean plane, with dihedral angles of 35.4° for S3−C5−S5−C7 and −101.9° for S4−C6−S6−C8 (Figure 2).

Bond lengths (Table 1) and angles are in agreement with the neutral state for the TTF unit. Note for both compounds the much shorter S2−C2 distance (1.717(3) Å for **3a** and 1.719(5) Å for **3b**) than the other outer S−C bonds in TTF, and longer C−N bonds next to the TTF unit (Table S1) than the four

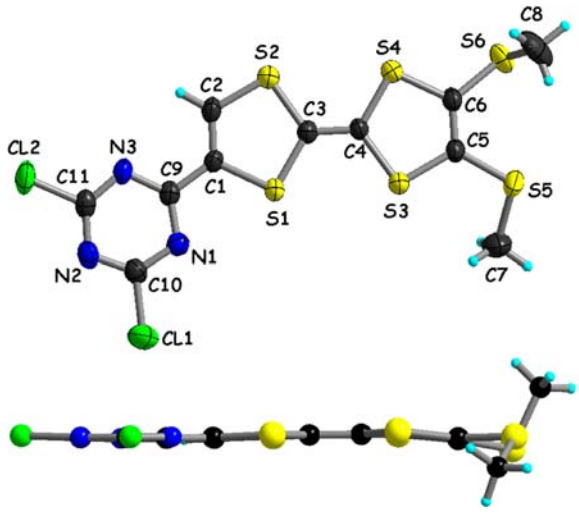

Figure 2. Molecular structure of **3b** with numbering scheme (top, ellipsoids at 50%), and a side view of the molecule (bottom).

other C−N bonds in TZ, are a likely consequence of the conjugation between the two units.

Although **3a** and **3b** are not isostructural, they present as a common feature the formation of head-to-tail centrosymmetric dyads, through the establishment of intermolecular S···S contacts of 3.80−3.93 Å and, especially, short D···A contacts as indicated by the centroid···centroid distances between the TZ ring and the S3−S4 dithiolene ring, amounting to 3.47 Å (**3a**) and 3.58 Å (**3b**), respectively (Figure 3). However, the shortest S···S intermolecular contacts develop laterally in the *ac* plane for **3a** (3.54 and 3.60 Å, Figure 4) and in the *bc* plane for **3b** (3.54 Å, Figure S4). Moreover, in the case of **3a**, unconventional hydrogen bonds N2···H6 (2.59 Å) are also observed, thus leading to an extended 2D structure.

Electrochemistry. Cyclic voltammograms (CV) of **1** and **2**, previously reported,[9] indicate two reversible oxidation processes, assigned to the two successive oxidations of the TTF groups, together with irreversible reductions of the TZ rings (Table 2). For the dichloro-TZ compounds **3a** and **3b**, the oxidation potentials of TTF are anodically shifted with respect to the dimethoxy-TZ compound **1**. This can be attributed to the enhanced electron acceptor character of the triazine ring in the former, as was also suggested by its more facile reduction, albeit irreversible. On the other hand, the CV of the tris(TTF) compound **4b** (**4a** was too insoluble for accurate electrochemical data) shows a very broad first oxidation peak at +0.59 V, clearly indicating the successive one-electron oxidation of the TTF units at very close potentials, and suggesting the possible evidence for mixed valence species (inset of Figure 5).

Absorption Behavior of the Neutral Compounds 3 and 4b. In the present family of D−A compounds, charge transfer is expected to occur as a transition from the TTF-based HOMO to the TZ-based LUMO, as noticed for **1** and **2**,[9] for which λ_{max} values of 492 and 530 nm, respectively, for the ^{1}ICT bands have been measured. The replacement of the methoxy groups in **1** by the electron-withdrawing chlorine substituents in **3** induces a massive red-shift of the ICT bands peaking now at 16 890 cm^{-1} (592 nm) with $\varepsilon = 3.3 \times 10^3$ M^{-1} cm^{-1} (**3a**) and 17 515 cm^{-1} (571 nm) with $\varepsilon = 3.5 \times 10^3$ M^{-1} cm^{-1} (**3b**) in DCM (Figure 6). Indeed, solutions of **3a** and **3b** in different solvents have blue-violet colors. The relative blue-shift of the

dx.doi.org/10.1021/ic3027336 | Inorg. Chem. 2013, 52, 5023−5034

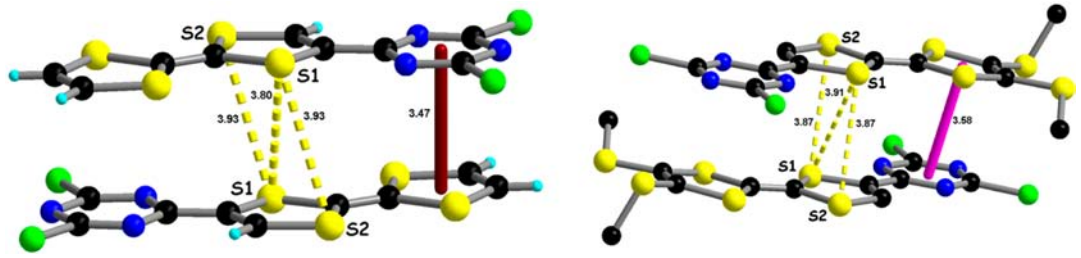

Figure 3. Centrosymmetric dimers in the solid-state structures of **3a** (left) and **3b** (right); distances: **3a** S1···S1($-x$, $1-y$, $-z$) 3.80 Å, S1···S2($-x$, $1-y$, $-z$) 3.93 Å; **3b** S1···S1($1+x$, y, $-1+z$) 3.91 Å, S1···S2($1+x$, y, $-1+z$) 3.87 Å.

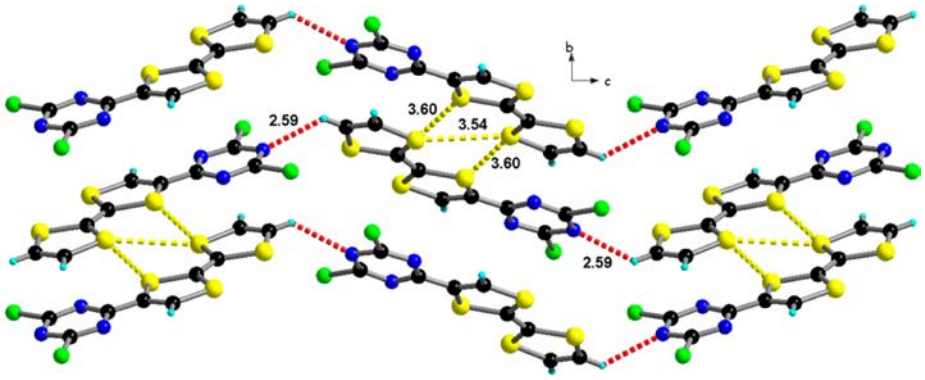

Figure 4. Packing of **3a** in the *bc* plane, with an emphasis on short lateral S···S contacts (S1···S3($1-x$, $-0.5+y$, $0.5-z$) 3.54 Å and S3···S3($1-x$, $-0.5+y$, $0.5-z$) 3.60 Å) and hydrogen bonds H6···N2($1+x$, $1.5-y$, $0.5+z$) 2.59 Å.

Table 2. Redox Potentials (V vs SCE) of Compounds 1, 2, and 4b in THF and of Compounds 3a,b in DCM/Acetonitrile

compound	$E_{1/2}^{ox1}$	$E_{1/2}^{ox2}$	E^{red}
1[a]	0.41	0.79	−1.98[b]
2[a]	0.43	0.76	−1.65[b]
3a[a]	0.54	0.96	−1.15[b]
3b[a]	0.60	0.92	−1.18[b]
4b[a]	0.59	0.87	−1.33[b]

[a]For comparison, potentials are converted to SCE by subtracting 0.04 V from measured Ag/AgCl values. [b]Irreversible process.

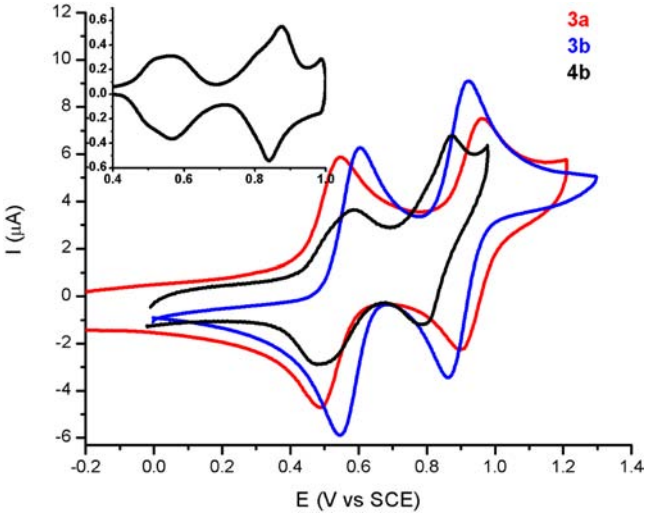

Figure 5. Cyclic voltammetry for **3a**, **3b** in dichloromethane (DCM)/acetonitrile (1:1) and **4b** in THF in the presence of (n-Bu_4N)PF_6 (0.1 M) at a scan rate of 0.1 V s^{-1}. Inset: Deconvoluted CV curve for **4b**.

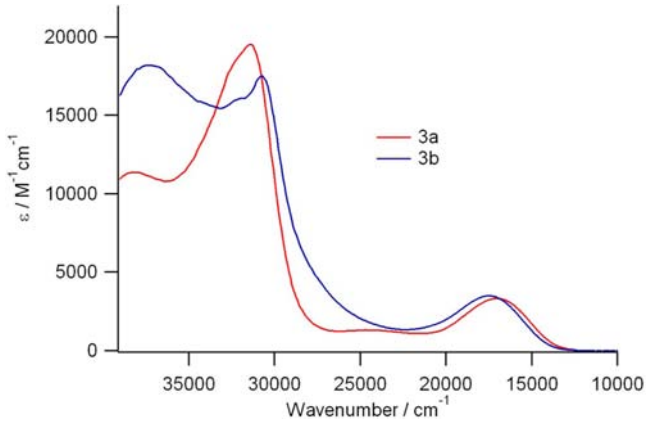

Figure 6. UV−vis absorption spectra of **3a** (red) and **3b** (blue) in DCM at room temperature (cell: 1 mm).

ICT band in **3b** with respect to **3a**, in agreement with the larger electrochemical gap of **3b** (vide supra), is very likely due to the slightly weaker donor character of the TTF unit resulting from the presence of the SMe groups. In the higher energy region, intense absorption bands are observed between 27 000 and 35 000 cm^{-1}, which can be ascribed to the TTF unit with extinction coefficients (ε) in the range of 1.7×10^4−1.9×10^4 M^{-1} cm^{-1}.

The large solubility of compound **3a** in a variety of organic solvents allowed a detailed study of its solvatochromic behavior. The absorption band of the ^{1}ICT transition of **3a** in several solvents with different polarities is shown in Figure 7. It is slightly red-shifted when going from nonpolar solvents (n-hexane, ν_{max} = 17 125 cm^{-1}; toluene, ν_{max} = 17 095 cm^{-1}) to intermediate polar solvents (DCM, ν_{max} = 16 890 cm^{-1}; chloroform, ν_{max} = 16 810 cm^{-1}). However, as the solvent

dx.doi.org/10.1021/ic3027336 | Inorg. Chem. 2013, 52, 5023−5034

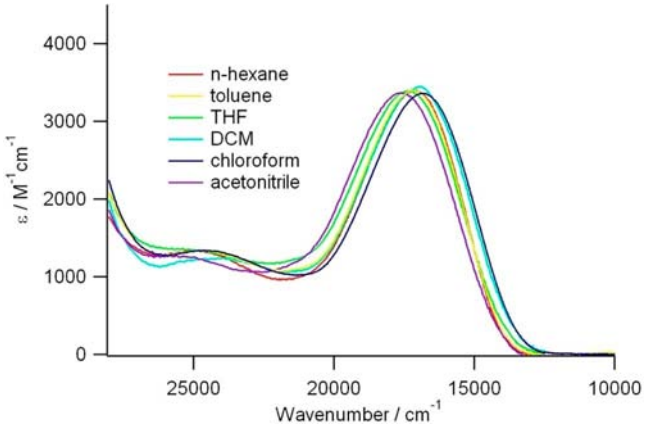

Figure 7. ^{1}ICT absorption band of **3a** (3×10^{-5} M) in different solvents.

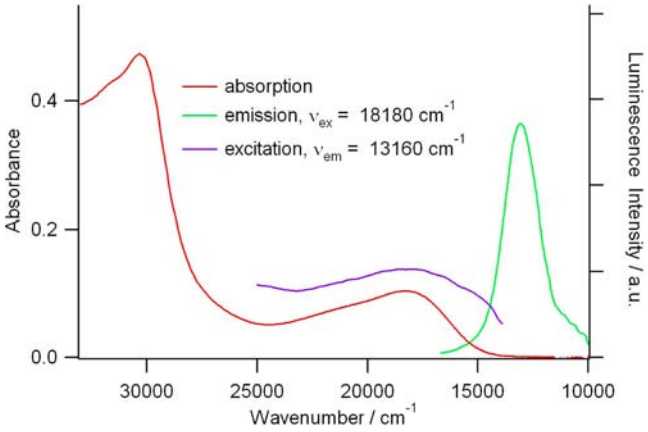

Figure 8. Absorption, emission, and excitation spectra of **4b** (9.0×10^{-6} M) in chloroform at room temperature.

polarity increases from DCM to acetonitrile, the CT absorption band is slightly blue-shifted, while a very large blue shift occurs in methanol (ν_{max} = 19 420 cm^{-1}), without any evident intermolecular aggregation (Figure S5). This observation is consistent with the cooperative effect of a polar ground state and hydrogen bonding. Such behavior induced by different solvents is also observed for **3b** (Figure S6).

The same variation of the solvatochromic behavior is observed for the bis(TTF) compound **2**, although its more limited solubility restrained the choice of solvents to toluene, DCM (slight red shift), and acetonitrile (slight blue shift) (Figure S7).

For the tris(TTF) compounds, only the more soluble SMe derivative **4b** could be investigated. Accordingly, the absorption spectrum of **4b** in chloroform (Figure S8a) shows intense absorption bands between 27 000 and 35 000 cm^{-1} ascribed to the TTF unit with extinction coefficients (ε) of the order of 3.4 $\times$ 10^4 M^{-1} cm^{-1}, and a very broad medium intensity band in the region between 13 000 and 25 000 cm^{-1} due to the ^{1}ICT transition. The ^{1}ICT absorption bands of **4b** in several solvents with different polarities (Figure S8b) show that, contrary to the mono(TTF) and bis(TTF) derivatives, the ^{1}ICT absorption band is continuously red-shifted from nonpolar solvents (cyclohexane, ν_{max} = 18 250 cm^{-1}) to intermediate polar solvents (DCM, ν_{max} = 18 280 cm^{-1}; chloroform, ν_{max} = 17 955 cm^{-1}), and then to highly polar solvents (acetonitrile, ν_{max} = 16 585 cm^{-1}; methanol, ν_{max} = 16 210 cm^{-1}).

Luminescence Study of 4b. Triazine derivatives with aryl, hydroxyl, methoxy, and amino substituents show fluorescence properties.[17] The mono(TTFs) **1** and **3** and the bis(TTF) **2** are no longer emissive, although **2** and **3** are photostable, as shown by the comparison between the absorption spectra before and after the emission−excitation experiments (Figures S9−S11). However, the tris(TTF) **4b** is weakly emissive in chloroform solution at room temperature. Upon excitation at ν = 18 180 cm^{-1}, a relatively broad emission centered at 13 055 cm^{-1} is observed (Figure 8), with a quantum efficiency of only 10^{-4} (Table 3). Because the excitation spectrum resembles the absorption spectrum in the region of the ^{1}ICT transition, it is safe to conclude that the emission actually results from the ^{1}ICT excited state. This is further borne out by the corresponding luminescence decay curve (Figure S12), which is close to the instrumental response, and thus gives a lifetime of less than 100 ps, in accordance with the low luminescence quantum efficiency. As for **1**, **2**, and **3**, photodecomposition of compound **4b** under oxygen-free conditions is slow (Figure S13); therefore, it can be considered as stable under light in the absence of oxygen. Attempts to record transient absorption spectra on the picosecond time scale following pulsed excitation failed due to the poor solubility.

Absorption Properties of the Oxidized Species. As mentioned above, one of the interesting features of TTF compounds concerns their reversible electrochromic properties, because the oxidized species show very distinct absorption properties.[3] Moreover, upon oxidation, the ^{1}ICT band of TTF−acceptor compounds is generally suppressed, and, consequently, a tuning of the luminescence properties can be achieved in some cases.[18] The oxidation process can be performed either spectroelectrochemically or chemically, in which case the appropriate choice of the oxidant is critical in terms of oxidative capacity and stability of the generated oxidized species in the presence of the oxidant and its reduced form. Figures 9 and 10 show the spectroelectrochemical oxidation of **3a** and **3b**, respectively, in DCM at room temperature. In the case of **3a**, absorption bands of the oxidized species appear in the range of 25 000−15 000 cm^{-1}, and can be readily attributed to the rapid formation of the radical cation TTF$^{+\bullet}$ (Figure 9),[19] with the concomitant decrease of the ^{1}ICT band. The two main absorptions, peaking at 22 620 cm^{-1} (442 nm) and 17 640 cm^{-1} (567 nm), can be attributed to SOMO→π^* and HOMO−1→SOMO transitions, respectively.[20] The same behavior is observed for the electrochemical oxidation of **1**, with ν_{max1} = 22 630 cm^{-1} (442 nm), ν_{max2} = 17 640 cm^{-1} (567 nm) (Figure S14).

On the other hand, the evolution of the absorption spectrum of **3b** shows a more gradual formation of the radical cation TTF$^{+\bullet}$ species, with bands at ν_{max1} = 23 040 cm^{-1} (434 nm) and ν_{max2} = 12 625 cm^{-1} (792 nm) concomitant with the disappearance of the original ^{1}ICT band. The red shift for the low energy band, with respect to **1** and **3a**, is due to the involvement of the external sulfur atoms in the composition of the HOMO−1 orbital, leading to a decrease of the HOMO−1−SOMO gap.[21]

Chemical oxidation of **1**, **3a**, and **3b** has been performed by the use of either $NOBF_4$, $[Fe(bpy)_3](PF_6)_3$, or $FeCl_3$ as oxidants (Figures S15−S25), and the same characteristic bands for the generated radical cations are observed as in the spectroelectrochemical experiments. Thus, the three oxidants achieve complete oxidation of the neutral mono(TTF) donors, yet the stability tests clearly show that the oxidized species are

dx.doi.org/10.1021/ic3027336 | Inorg. Chem. 2013, 52, 5023−5034

Table 3. Photophysics for $(TTF)_3$-TZ 4b at Room Temperature

compound	solvent	ν_{abs}/cm^{-1} (ε/M^{-1} cm^{-1})	ν_{em}/cm^{-1}	Φ_f	τ/ns
4b	$CHCl_3$	37 175 (32 800), 30 305 (34 800), 17 955 (7600)	13 055	0.00011	<0.10

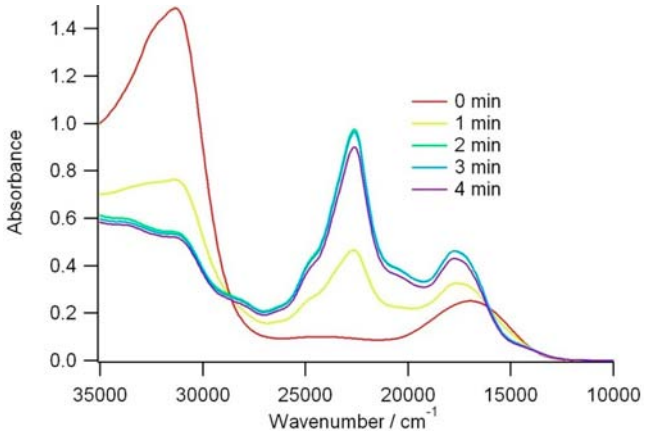

Figure 9. UV−vis absorption spectra of **3a** (5×10^{-4} M) during electrochemical oxidation at 0.30 V vs a Ag wire pseudo reference electrode (corresponds to 0.73 V vs SCE) in DCM at room temperature, cell length: 0.7 mm.

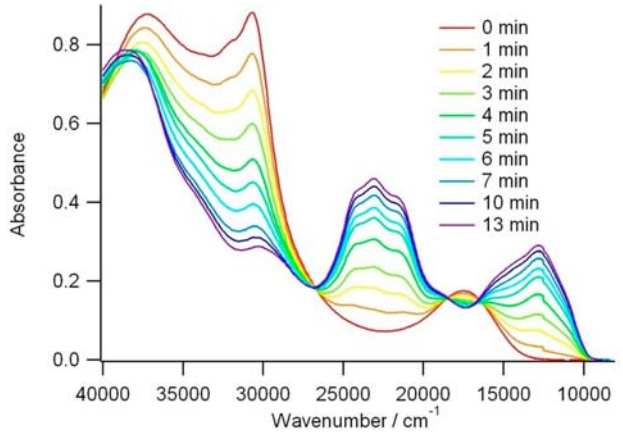

Figure 10. UV−vis absorption spectra of **3b** (7.6×10^{-4} M) during electrochemical oxidation at 0.55 V vs an Ag wire pseudo reference (corresponds to 0.69 V vs SCE) in DCM at room temperature, cell length: 0.7 mm.

unstable and easily degrade upon using $NOBF_4$, while they are stable for the two other oxidants.

The oxidation of the bis(TTF) compound **2** has been performed electrochemically (Figure S26) and chemically with $[Fe(bpy)_3](PF_6)_3$ (Figure S27) or $FeCl_3$ (Figure 11). Stable oxidized species, absorbing between 25 000 and 15 000 cm^{-1}, are generated. The fate of the ^{1}ICT band[9] at 18 900 cm^{-1} is somewhat more difficult to discern, but taking into account the intense new bands on either side, its contribution to the absorption at that energy is decreasing in accordance with the other compounds of the series. While adding 0.0−1.0 equiv of $FeCl_3$, one of the two TTF units per molecule is gradually oxidized to the radical cation. The second TTF unit is then oxidized by the subsequent additions of equivalents of $FeCl_3$. No intervalence low energy band could be detected during the oxidation for the intermediate species.

Oxidation of the tris(TTF) **4b** has been achieved chemically by the use of $FeCl_3$ (Figure 12) or $NOBF_4$ (Figure S28). The

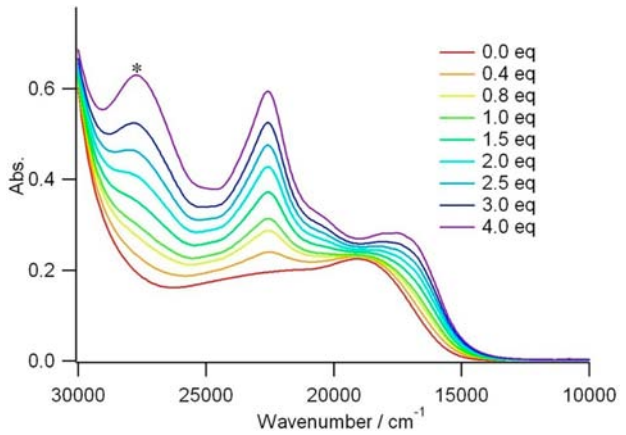

Figure 11. UV−vis absorption spectra of **2** (5×10^{-5} M) during chemical oxidation by successive addition of $FeCl_3$ in DCM at room temperature; "*" represents unreacted $FeCl_3$.

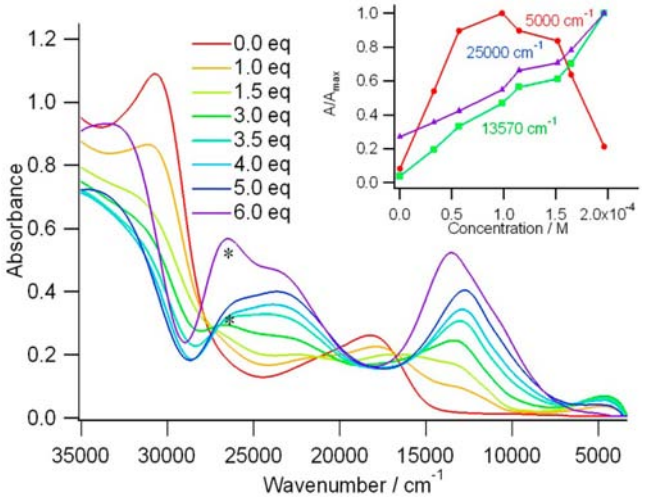

Figure 12. UV−vis absorption spectra of **4b** (3.3×10^{-5} M) during chemical oxidation by successive addition of the oxidant $FeCl_3$ in chloroform at room temperature. Inset: Absorbance changes at different wavenumbers by successive addition of oxidant $FeCl_3$ at room temperature.

chemical oxidation process seems complete after adding 6 equiv of $FeCl_3$, and formation of radical cation species is suggested by the decrease in intensity of the ^{1}ICT band and the new bands at 13 570 and 25 000 cm^{-1} typical for $TTF^{+\bullet}$.[19] The oxidized species are stable and hardly degraded in chloroform solution at room temperature when $FeCl_3$ is added as oxidant (Figure S29). Interestingly, a new band appears at around 5000 cm^{-1} (2000 nm) during the oxidation. This band shows a different dependence upon successive addition of oxidant from the two bands of $TTF^{+\bullet}$, appearing at ν_{max1} = 25 000 cm^{-1} (400 nm) and ν_{max2} = 13 570 cm^{-1} (737 nm). These increase continuously in intensity, whereas the band at 5000 cm^{-1} reaches a maximum at 1 equiv of oxidant added and then decreases again to completely disappear when full oxidation of the three TTFs is achieved. This absorption band is very likely representative of a coupling between TTF and $TTF^{+\bullet}$ moieties

dx.doi.org/10.1021/ic3027336 | Inorg. Chem. 2013, 52, 5023−5034

Table 4. Calculated Energies (eV) and Mulliken Composition (%) of Frontier Orbitals of Neutral Forms[a]

	(R_1 = H,R_2 = H) (C_s) model		(R_1 = Cl,R_2 = H) (C_s) **3a**		(R_1 = OMe,R_2 = H) (C_1) **1**		(R_1 = Cl,R_2 = SMe) (C_1) **3b**	
MO	TTF/TZ/R_1	eV	TTF/TZ/R_1	eV	TTF/TZ/R_1	eV	TTFSMe$_2$/TZ/R_1	eV
LUMO+4	98/2/0	−0.26	98/2/0	−0.44	75/20/0	−0.23	100/0/0	−0.67
LUMO+3	97/3/0	−0.50	96/3/0	−0.65	36/55/9	−0.45	100/0/0	−1.31
LUMO+2	100/0/0	−1.14	100/0/0	−1.32	89/9/2	−0.47	99/1/0	−1.33
LUMO+1	2/96/2	−1.55	2/85/13	−1.88	100/0/0	−0.99	2/85/13	−1.92
LUMO	43/57/0	−2.28	42/55/2	−2.66	49/49/2	−1.94	42/55/2	−2.69
HOMO	97/3/0	−4.99	97/3/0	−5.17	98/2/0	−4.97	97/3/0	−5.35
HOMO−1	93/7/0	−7.02	93/6/0	−7.22	92/7/0	−6.87	97/3/0	−6.86
HOMO−2	7/88/5	−8.03	94/5/1	−8.37	66/26/8	−7.95	100/0/0	−7.10
HOMO−3	4/94/2	−8.13	11/82/7	−8.61	6/77/17	−8.05	97/3/0	−7.56
HOMO−4	93/7/0	−8.17	87/10/2	−8.67	19/65/16	−8.07	96/4/0	−8.17

[a] R_1, substituent on TZ; R_2, substituent on TTF.

and hence can be attributed to an intervalence transition.[22] The same behavior is observed when $NOBF_4$ is used as oxidant. Because for the mono and bis(TTF) compounds this low energy band was not observed, its assignment to an intramolecular rather to an intermolecular charge transfer transition seems likely. However, once again, when oxidation is performed with $NOBF_4$, the oxidized species are unstable and degrade within less than 1 h (Figure S30).

The photophysical study of all of the chemically oxidized derivatives indicates that none of the oxidized species is emissive. This observation is particularly interesting in the case of the tris(TTF) **4b**, which is luminescent in its neutral form and then the luminescence is quenched upon oxidation. Although in the present case the electrochemical reversibility of the photophysical properties was not actually checked, the CV data indicate that the first oxidation−reduction cycle of **4b** is fully reversible. By comparison with a Pt(II) complex having an analogous TTF unit incorporated into a bidentate ligand, for which the spectroelectrochemical reversibility of the TTF oxidation was found to be quantitative,[23] it may be safely inferred that this is also the case for **4b** given its comparative chemical stability in the oxidized form. This also holds for the other systems.

DFT Calculations for 1 and 3. To further characterize the nature of the electronic transitions observed for the TTF-triazine compounds described herein, DFT calculations[24] have been performed at the DFT/PBE0 level for the geometry optimizations and the TDDFT/PBE0[25] level for the electronic transitions, with the Gaussian 09[26] program package. Previously, theoretical calculations at the DFT/B3LYP level for the neutral **1** and **2** allowed the unambiguous assignment of the ICT bands to $\pi_{HOMO} \rightarrow \pi^*_{LUMO}$ excitations with the HOMO based on the TTF unit and the LUMO on the TZ ring.[9] Note that two ICT bands were calculated for the bis(TTF) **2** because of the quasi-degeneracy of the HOMO and HOMO−1 orbitals, with a λ_{max} red-shifted with respect to the mono(TTF) **1**, in agreement with the experimental UV−vis spectra. In the present study, the neutral and cationic forms of the new mono(TTF) derivatives **3a** and **3b** are investigated, together with compound **1** for comparison and the model compound TTF-TZ, with H atoms instead of Cl or MeO groups on the TZ ring. Moreover, neutral, monocationic, and dicationic forms of the tris(TTF) **4a** are also investigated.

Optimized geometries for **1**, **3a**, and **3b** are in agreement with the experimental X-ray structures and reproduce, for example, the coplanarity between the TTF and TZ units, which is thus not the consequence of the solid-state packing. The relative energies of the frontier orbitals (Table 4), which are as expected π $HOMO_{TTF}$ and π^* $LUMO_{TZ}$, although in the latter the neighboring dithiole ring has an important contribution (Figure 13 and Table S7), clearly suggest that the donor **1**

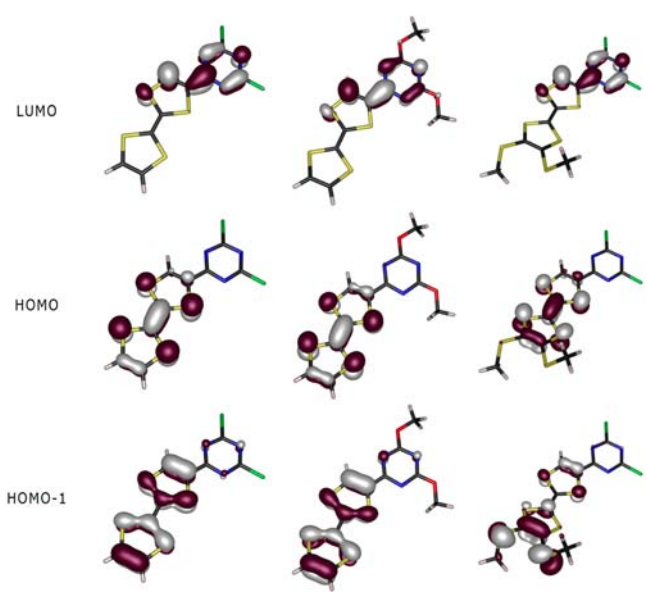

Figure 13. Frontier orbitals for **3a** (left), **1** (middle), and **3b** (right).

oxidizes most readily, followed by **3a**, and then **3b**, according to the positions of the HOMOs and in agreement with the electrochemical data (see Table 2), while the reduction of the TZ ring is much more favorable for the chlorinated derivatives **3a** and **3b** than for the methoxy compound **1**, as indicated by the positions of the LUMOs. The relative influence of the TZ substituents is suggestive when also considering the energies of the orbitals of the parent TTF-TZ, which is expected to have an intermediate reduction potential between **1** and **3**. Moreover, the HOMO−LUMO gap is much larger for **1** (3.03 eV) than for **3a** (2.51 eV) and **3b** (2.66 eV), in agreement with the bathochromic shift of the ICTs bands of **3a** and **3b** with respect to **1**, while between **3a** and **3b** the gap slightly increases, in accordance with the experimental blue shift of the ICT band in the latter with respect to the former.

Vertical excitations were calculated on the optimized ground-state geometries of the four compounds at the TDDFT level. In all cases, the lowest energy singlet transitions correspond to the $\pi_{HOMO} \rightarrow \pi^*_{LUMO}$ excitations, and are predicted to be at 18 388

dx.doi.org/10.1021/ic3027336 | Inorg. Chem. 2013, 52, 5023−5034

Table 5. TD-DFT Energies and Assignment of the Most Pertinent Low-Lying Electronic Excitations of 3a

wavenumber/cm^{-1}	λ/nm	osc.	symmetry	assignment	transition
14 756	678	0.080	singlet-A′	TTF→TZ/TTF	HOMO→LUMO (99%)
21 540	464	0.040	singlet-A′	TTF→TZ	HOMO→LUMO+1 (99%)
31 903	313	0.193	singlet-A′	TTF→TZ/TTF	HOMO−1→LUMO (96%)
34 183	293	0.387	singlet-A′	TTF→TTF	HOMO→LUMO+4 (95%)
39 818	251	0.267	singlet-A′	TTF→TZ/TTF	HOMO−2→LUMO (83%)

Table 6. TD-DFT Energies and Assignment of the Most Pertinent Low-Lying Electronic Excitations of 3b[a]

wavenumber/cm^{-1}	λ/nm	osc.	symmetry	assignment	transition
15 889	629	0.083	singlet-A	TTF→TZ/TTF	HOMO→LUMO (99%)
29 248	342	0.091	singlet-A	TTF→TZ/TTF	HOMO−1→LUMO (97%)
32 046	312	0.136	singlet-A	TTF→TTF	HOMO→LUMO+4/+5/+6 (68%)
32 992	303	0.276	singlet-A	TTF→TTF	HOMO→LUMO+5/+4/+6 (80%)
38 750	258	0.146	singlet-A	TTF→TZ/TTF	HOMO−4→LUMO (55%)
					HOMO−2→LUMO+1 (24%)

[a]For a full description of all transitions and a graphical representation of the calculated versus experimental spectra, see the Supporting Information.

cm^{-1} (544 nm) for **1**, 14 756 cm^{-1} (678 nm) for **3a**, 15 889 cm^{-1} (629 nm) for **3b**, and 16 165 cm^{-1} (619 nm) for the parent TTF-TZ, with oscillator strengths f in the range 0.065−0.083 (Tables 5 and 6 and Tables S8,S9). The calculated values for the electronic transitions reproduce the experimental spectra and are in agreement with the variation of the ICT band with the substituent scheme on TZ and TTF units.

Radical cation forms have been calculated for **1** and **3a**. The spin density maps indicate delocalization of the unpaired electron on the TTF unit (Figure S33). TDDFT results for the vertical excitations show that the lowest energy transitions for **1**$^{+\bullet}$ and **3a**$^{+\bullet}$, although appearing at very close values, that is, 18 585 cm^{-1} (538 nm) and 19 395 cm^{-1} (516 nm), respectively, in agreement with the experimental λ_{max} value of 567 nm, differ in their origin (Tables S12,S13). Indeed, for **1**$^{+\bullet}$, this excitation, with f of 0.090, corresponds to a pure TTF→TTF (HOMO/−2/−3β→LUMOβ) transition, while for **3a**$^{+\bullet}$ (f = 0.111), it is a combination of TTF→TTF (HOMOβ→LUMOβ) and TTF→TZ/TTF (HOMOα→LUMOα) transitions, the latter being reminiscent of the ICT. In **1**$^{+\bullet}$, this excitation appears at slightly higher energy as an independent transition, following the relative positions of the TZ-based LUMOα, determined by the nature of the substituents, as was already discussed for the neutral compounds. For both compounds, the more intense transitions at 26 082 cm^{-1} (**1**$^{+\bullet}$) and 25 662 cm^{-1} (**3a**$^{+\bullet}$), to be compared to the experimental values of 22 630 cm^{-1} (**1**$^{+\bullet}$) and 22 620 cm^{-1} (**3a**$^{+\bullet}$), then correspond to TTF→TTF (HOMOα→LUMOα+2) excitations.

DFT Calculations for 4a. DFT and TDDFT calculations have been undertaken on neutral, cationic, and dicationic forms of **4a**, thus without the SMe substituents on TTF as in **4b**, to avoid the conformational issues and the increase of the computational time. The composition of the frontier orbitals shows that the HOMO is equally distributed on the three TTF units, and the HOMO−1 and HOMO−2, which are degenerated, contain more contribution of two out of three TTFs (Figure 14 and Table 7). LUMO and LUMO+1 are degenerated and contain mainly TZ contribution.

Vertical excitations were calculated on the optimized ground-state geometry of C_s symmetry, at the TDDFT level. As shown in Table 8, there are two ICT transitions both doubly degenerated, at 15 782 cm^{-1} (634 nm) and 17 040 cm^{-1} (587 nm) corresponding to $\pi_{HOMO/-1/-2}\rightarrow\pi^*_{LUMO/+1}$ excitations, with oscillator strengths f of 0.112 and 0.111, respectively, in agreement with the very broad experimental absorption band peaking at 17 954 cm^{-1} (557 nm). The next more intense band at higher energies then results from a superposition of strong intensity transitions assigned to TTF→TZ/TTF (ICT) and TTF→TTF excitations (Figure 15).

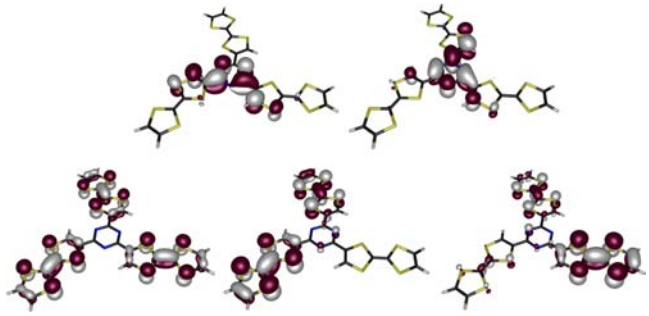

Figure 14. Frontier orbitals representation of ^{1}TZ-TTF$_3$ (C_s) **4a** with an isovalue of 0.03: LUMO (top left), LUMO+1 (top right), HOMO (bottom left), HOMO−1 (bottom middle), HOMO−2 (bottom right).

Table 7. Calculated Energies (eV) and Mulliken Composition (%) of Frontier Orbitals of 4a (C_s)

MO	TZ/TTF1/TTF2/TTF3	eV
LUMO+5	13/29/29/29	−0.96
LUMO+4	0/33/33/33	−1.05
LUMO+3	0/40/60/0	−1.06
LUMO+2	0/30/8/68	−1.06
LUMO+1	53/30/6/11	−2.30
LUMO	53/1/26/21	−2.30
HOMO	1/33/33/33	−4.91
HOMO−1	4/39/56/2	−4.97
HOMO−2	4/25/8/62	−4.97
HOMO−3	9/63/27/1	−6.96
HOMO−4	9/12/41/38	−6.96
HOMO−5	2/18/25/54	−6.96

Then monocationic and dicationic species of **4a** have also been calculated (Tables S14−S17), especially to theoretically support and characterize the near-infrared band at around 2000 nm observed during the chemical oxidation of **4b**. Spin density

dx.doi.org/10.1021/ic3027336 | Inorg. Chem. 2013, 52, 5023−5034

Table 8. TD-DFT Calculated Energies and Assignment of the Most Pertinent Low-Lying Electronic Excitations of Neutral 4a

wavenumber/ cm^{-1}	λ/ nm	osc.	symmetry	assignment	transition
15 782	634	0.112	doubly degenerate singlet-A′	TTFs→TZ/TTF	HOMO/−1/−2→LUMO (88%) HOMO/−1/−2→LUMO+1 (88%)
17 040	587	0.111	doubly degenerate singlet-A′	TTFs→TZ/TTF	HOMO/−1/−2→LUMO/+1 (99%) HOMO/−1/−2→LUMO/+1 (99%)
27 207	368	0.030	doubly degenerate singlet-A′	TTF→TTF	HOMO−1→LUMO+5 (89%) HOMO−2→LUMO+5 (89%)
32 369	309	0.464	doubly degenerate singlet-A′	TTFs→TZ/TTF	HOMO−4/−3/−5→LUMO+1 (80%) HOMO−5/−3/−4→LUMO+1 (83%)
32 984	303	0.153	doubly degenerate singlet-A′	TTFs→TZ/TTF	HOMO−5/−4/−3→LUMO+1 (78%) HOMO−5/−3/−4→LUMO+1 (88%)
34 400	291	0.298	doubly degenerate singlet-A′	TTF→TTF	HOMO/−1/−2→L+9/+8/+11 (57%) HOMO/−2/−1→L+10/+8/+11 (61%)
34 567	289	0.103	doubly degenerate singlet-A′	TTF→TTF	HOMO−1→LUMO+8 (43%) HOMO−2→LUMO+8 (43%)

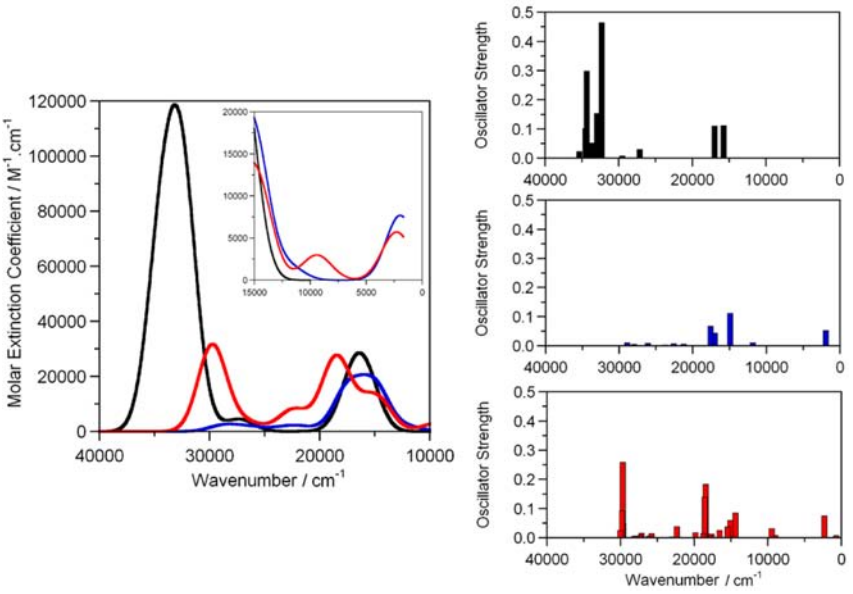

Figure 15. On the left side, theoretical absorption spectra of neutral (black), cation (blue), and dication (red) forms of **4a**. On the right side, electronic transitions (neutral, top; cation, middle; dication, bottom).

maps of $\mathbf{4a}^{+\bullet}$ and $\mathbf{4a}^{2+}$ triplet state (more stable than the singlet) show uniform repartition on the three TTF units (Figure S36). Vertical excitation calculations indicate that both monocationic and dicationic species possess very low energy TTF→TTF intervalence transitions at 1968 cm^{-1} (5082 nm) (f = 0.053) and 2370 cm^{-1} (4219 nm) (f = 0.075), respectively. This supports the stepwise formation of $\mathbf{4b}^{+\bullet}$ and $\mathbf{4b}^{2+}$ and their detection through the experimental NIR absorption band peaking at 5000 cm^{-1} (vide supra). Note that these results are in accordance with the electrochemical study of **4b** for which the first oxidation process is very broad, as a consequence of the three successive monoelectronic oxidation steps. The next excitations then correspond to reminiscent ICT for both species, while the higher energy transitions are internal TTF→TTF excitations, typical for $TTF^{+\bullet}$ (Figure 15). Interesting to note is the existence of an ICT at 9530 cm^{-1} (1049 nm) in the calculated spectrum of $\mathbf{4a}^{2+}$, which could provoke the broadening of the experimental band appearing between 10 000 and 15 000 cm^{-1}, when 1−3 equiv of oxidant has been added (see Figure 12 and Figure S29). One can thus infer that the first equivalent of oxidant produces the radical cation $\mathbf{4b}^{+\bullet}$, then the oxidation becomes more difficult and 2 more equiv of oxidant is required to generate the dication $\mathbf{4b}^{2+}$, while the formation of the trication, accompanied by the disappearance of the NIR band, is complete when 6 equiv of $FeCl_3$ is added.

Crystalline Radical Cation Salt [(3a)(PF_6)]. As a confirmation of the stability of the oxidized species of the TTF-triazine derivatives and their propensity to serve as precursors for radical cation salts, we have prepared by electrocrystallization a first crystalline radical cation salt of **3a** with the PF_6^- anion. Black prism-shaped crystals have been collected on the electrode, and also from the anodic compartment of the cell after two weeks. The salt is formulated as [(**3a**)(PF_6)], and it crystallizes in the monoclinic system, space group $P2_1/n$, with one independent molecule of donor and anion in the unit cell (Figure S37). Therefore, each TTF has a charge +1, which is in agreement with the analysis of the bond lengths (Table 1 and Table S1) showing a significant increase to 1.384(8) Å of the central C3═C4 bond, to compare with 1.344(4) Å for the neutral **3a** (see Table 1), and an average of 1.720 Å for the internal S−C bonds (1.761 Å for **3a**). The radical cations of **3a** form eclipsed centrosymmetric dimers at the supramolecular level, with short S···S intermolecular contacts of 3.43 and 3.47 Å. Furthermore,

dx.doi.org/10.1021/ic3027336 | Inorg. Chem. 2013, 52, 5023−5034

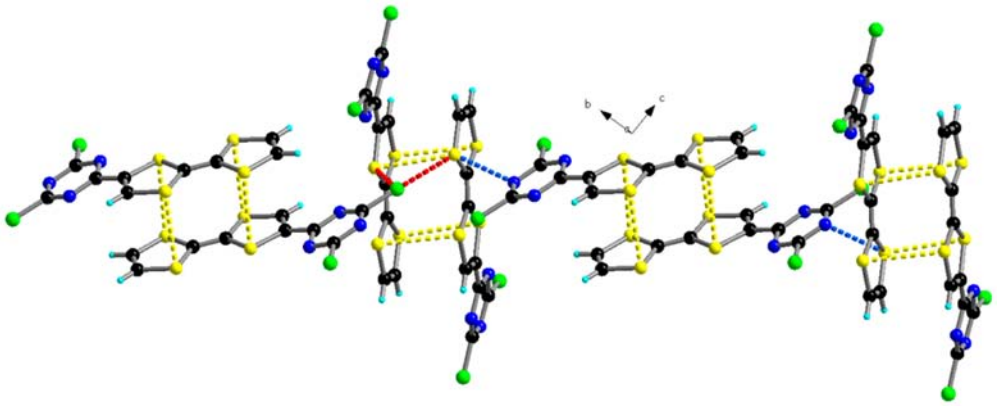

Figure 16. Packing of $[(\mathbf{3a})(PF_6)]$, with an emphasis on the short S···S contacts (3.43 and 3.47 Å, highlighted in yellow) within the centrosymmetric dimers, Cl···S contacts (3.56 and 3.66 Å, highlighted in red), and N···S contacts (3.14 Å, highlighted in blue). PF_6^- anions have been omitted.

these dimers interact in the *bc* plane through N···S (3.14 Å) contacts and along the *a* direction through Cl···S (3.56 and 3.66 Å) intermolecular interactions, thus establishing a 3D structure (Figure 16). No classical organic−inorganic segregation is observed, because the anions are located in the interstices between the dimers (Figure S38).

As a consequence of the strong dimerization of the TTF radical cations in the solid state, no electron delocalization is expected to occur. However, the preparation of this first radical cation salt within the family of TTF-TZ donor−acceptor compounds clearly points out the interest of these derivatives not only for their electrochromic and tunable emissive behavior in solution, but also as precursors for crystalline radical cation or charge transfer salts, possibly provided with conducting properties, in which the classical TTF···TTF interactions compete with the specific TTF···TZ interactions.

CONCLUSIONS

The (mono)TTF-TZ **1**, **3a**, and **3b**, (bis)TTF-TZ **2**, and (tris)TTF-TZ **4a** and **4b** donor−acceptor compounds have been efficiently synthesized by palladium cross-coupling reactions. Single-crystal X-ray analyses show planar structures in the solid state for **3a** and **3b**, which organize in centrosymmetric dimers through the establishment of short intermolecular D···A contacts. The ICT band is evidenced in all of the compounds and corresponds to a charge transfer from the TTF to the TZ ring as a $\pi(\mathrm{HOMO_{TTF}})\rightarrow\pi^*(\mathrm{LUMO_{TZ}})$ excitation. The position of the ICT band is red-shifted when the electron-withdrawing chlorine substituents replace the methoxy groups on the TZ ring. Photophysical investigations evidenced the emissive properties of the C_3 symmetric tris(TTF) **4b**, the luminescence being quenched upon oxidation. The radical cation species have been spectroscopically and theoretically characterized. All of the radical cations are stable except in the oxidation conditions with $NOBF_4$, the use of which should thus be considered with great care in TTF−acceptor compounds. Interestingly, the ICT band still exists in the radical cations, but it is generally superposed to the internal $TTF^{+\bullet}$ transition. During the chemical oxidation of **4b**, clear evidence for intervalence transitions in the radical cation and dication species is provided. TD DFT calculations show indeed the occurrence of such transition in both species. All of these D−A compounds constitute valuable precursors for solid-state materials either in the neutral state, upon activation of the charge mobility by irradiation in the ICT band, or in the oxidized radical cation or charge transfer salts. A solid argument in this direction is provided by the preparation and structural characterization of the radical cation salt $[(\mathbf{3a})^{+\bullet}(PF_6)^-]$. Moreover, depending on the substitution scheme on triazine, switchable luminescent systems may be achieved.

EXPERIMENTAL SECTION

General. Reactions were carried out under argon and using toluene HPLC. Nuclear magnetic resonance spectra were recorded on a Bruker Avance DRX 500 spectrometer (operating at 500.04 MHz for ^1H and 125 MHz for ^{13}C) and Bruker Avance DRX 300 automatic spectrometer (operating at 300 MHz for ^1H and 75 MHz for ^{13}C). Chemical shifts are expressed in parts per million (ppm) downfield from external tetramethysilane, $Si(CH_3)_4$. The following abbreviations are used: s, singlet; d, doublet. UV−vis spectra were recorded in solution using a Lambda 19 PERKIN ELMER spectrometer. MALDI-TOF mass spectra were recorded on Bruker Biflex-IIITM apparatus, equipped with a 337 nm N_2 laser. Elemental analyses were recorded using a Flash 2000 Fisher Scientific Thermo Electron analyzer.

Syntheses. 4-(Trimethylstannyl)-tetrathiafulvalene and 4-(trimethylstannyl)-4′,5′-bis(methylthio)-tetrathiafulvalene were synthesized according to a procedure previously described.[15]

*TTF-TZ-(MeO)$_2$ (**1**).* 2-Chloro-4,6-dimethoxy-1,3,5-triazine (0.10 g, 0.56 mmol), 4-(trimethylstannyl)-tetrathiafulvalene (0.25 g, 0.68 mmol), and $Pd(PPh_3)_4$ (118 mg, 15% mmol) as catalyst were mixed in 20 mL of dry toluene and refluxed for 12 h under argon. The mixture was filtered over Celite and silica, washed with toluene and dichloromethane, and dried under vacuum. The residue was purified by column chromatography (dichloromethane) to give 150 mg of red powder, yield: 78%. ^1H NMR (500 MHz, $CDCl_3$) δ/ppm: 7.81 (s, 1H), 6.34 (d, $^3J_{HH}$ = 6.2 Hz, 1H), 6.32 (d, $^3J_{HH}$ = 6.2 Hz, 1H), 4.06 (s, 6H). ^{13}C NMR (125 MHz, $CDCl_3$) δ/ppm: 172.3, 167.8, 134.9, 119.3, 118.7, 113.2, 108.3, 55.4. MS (EI$^+$-DSQ) *m*/*z*: 342.96 (M_{th} = 342.96). Anal. Calcd for $C_{11}H_9N_3O_2S_4$: C, 38.47; H, 2.64; N, 12.23. Found: C, 38.71; H, 2.44; N, 11.97.

*(TTF)$_2$-TZ-MeO (**2**).* 2,4-Dichloro-6-dimethoxy-1,3,5-triazine (84 mg, 0.49 mmol), 4-(trimethylstannyl)-tetrathiafulvalene (0.5 g, 1.4 mmol), and $Pd(PPh_3)_4$ (240 mg, 15% mmol) as catalyst were mixed in 20 mL of dry toluene and refluxed for 12 h under argon. The mixture was diluted with THF, filtered, and concentrated to one-half of the volume. Cyclohexane was added, and the mixture was kept overnight in the refrigerator to afford 190 mg of dark purple crystalline powder, yield: 75%. ^1H NMR (500 MHz, THF-d_8) δ/ppm: 8.07 (s, 2H), 6.57 (d, $^3J_{HH}$ = 6.2 Hz, 2H), 6.54 (d, $^3J_{HH}$ = 6.2 Hz, 2H), 4.06 (s, 3H). MS (MALDI-TOF) *m*/*z*: 514.84 (M_{th} = 514.85). Anal. Calcd for $C_{16}H_9N_3OS_8$: C, 37.26; H, 1.76; N, 8.15. Found: C, 36.91; H, 1.95; N, 8.01.

*TTF-TZ-Cl$_2$ (**3a**).* 2,4,6-Trichloro-1,3,5-triazine (1.04 g, 5.44 mmol), 4-(trimethylstannyl)-tetrathiafulvalene (0.5 g, 1.36 mmol), and

dx.doi.org/10.1021/ic3027336 | *Inorg. Chem.* 2013, 52, 5023−5034

$Pd(PPh_3)_4$ (235 mg, 15% mmol) as catalyst were mixed in 80 mL of dry toluene and refluxed for 12 h under argon. The mixture was filtered over Celite and silica, washed with toluene and dichloromethane, and dried under vacuum. The residue was purified by column chromatography (cyclohexane/dichloromethane 1/1) to give 300 mg of black solid, yield: 62%. ^{1}H NMR (500 MHz, CD_2Cl_2) δ/ppm: 8.12 (s, 1H), 6.41 (d, $^3J_{HH}$ = 6.0 Hz, 1H), 6.39 (d, $^3J_{HH}$ = 6.0 Hz, 1H). ^{13}C NMR (125 MHz, CD_2Cl_2) δ/ppm: 171.8, 167.1, 137.6, 133.1, 119.9, 119.5, 116.5, 106.71. MS (MALDI-TOF) m/z: calcd for $C_9H_3Cl_2N_3S_4$ 350.85, found 350.30. Anal. Calcd for $C_9H_3Cl_2N_3S_4$: C, 30.68; H, 0.86; N, 11.93; S, 36.41. Found: C, 30.98; H, 0.95; N, 11.65; S, 36.14.

*$(SMe)_2$TTF-TZ-Cl_2 (**3b**).* 2,4,6-Trichloro-1,3,5-triazine (90 mg, 0.49 mmol), 4-(trimethylstannyl)-4′,5′-bis(methylthio)-tetrathiafulvalene (225 mg, 0.49 mmol), and $Pd(PPh_3)_4$ (75 mg, 15% mmol) as catalyst were mixed in 20 mL of dry toluene and refluxed for 12 h under argon. The mixture was filtered over Celite and silica, washed with toluene and dichloromethane, and dried under vacuum. The residue was purified by column chromatography (cyclohexane/dichloromethane 4/1) to give 160 mg of black solid, yield: 73%. ^{1}H NMR (300 MHz, $CDCl_3$) δ/ppm: 8.10 (s, 1H), 2.43 (s, 3H), 2.42 (s, 3H). ^{13}C NMR (125 MHz, CD_2Cl_2) δ/ppm: 171.9, 167.1, 137.2, 132.9, 128.6, 127.6, 125.5, 112.1, 19.6. MS (MALDI-TOF) m/z: calcd for $C_{11}H_7Cl_2N_3S_6$ 442.83, found 443.50. Anal. Calcd for $C_{11}H_7Cl_2N_3S_6$: C, 29.72; H, 1.59; N, 9.45; S, 42.28. Found: C, 30.03; H, 1.79; N, 9.17; S, 42.54.

*$(TTF)_3$-TZ (**4a**).* 2,4,6-Trichloro-1,3,5-triazine (55.8 mg, 0.3 mmol), 4-(trimethylstannyl)-tetrathiafulvalene (367 mg, 1 mmol), and $Pd(PPh_3)_4$ (173 mg, 15% mmol) as catalyst were mixed in 30 mL of dry toluene and refluxed overnight under argon. The mixture was filtered, and the black solid was washed several times with toluene, dichloromethane, acetone, and methanol. Yield: 30%. ^{1}H NMR (300 MHz, THF-d_8) δ/ppm: 8.17 (s, 1H), 6.59 (d, 2H). MS (MALDI-TOF) m/z: calcd for $C_{21}H_9N_3S_{12}$ 686.84, found 686.60. Anal. Calcd for $C_{21}H_9N_3S_{12}$: C, 36.66; H, 1.32; N, 6.11; S, 55.92. Found: C, 36.84; H, 1.58; N, 5.94; S, 55.60.

*[$(SMe)_2$TTF]$_3$-TZ (**4b**).* 2,4,6-Trichloro-1,3,5-triazine (42.6 mg, 0.23 mmol), 4-(trimethylstannyl)-4′,5′-bis(methylthio)-tetrathiafulvalene (350 mg, 0.76 mmol), and $Pd(PPh_3)_4$ (130 mg, 15% mmol) as catalyst were mixed in 30 mL of dry toluene and refluxed overnight under argon. The mixture was filtered over Celite and silica, washed with toluene, dichloromethane, and chloroform, and dried under vacuum. The black residue was washed several times with methanol and then extracted with hot chloroform to give a black solid. Yield: 55%. ^{1}H NMR (300 MHz, $CDCl_3$) δ/ppm: 7.88 (s, 1H), 2.46 (s, 3H), 2.44 (s, 3H). MS (MALDI-TOF) m/z: calcd for $C_{27}H_{21}N_3S_{18}$ 960.67, found 962.30. Anal. Calcd for $C_{27}H_{21}N_3S_{18}$: C, 33.62; H, 2.19; N, 4.36; S, 59.83. Found: C, 33.92; H, 2.14; N, 4.23; S, 59.48.

*[(**3a**)(PF_6)].* 27.5 mg (0.071 mmol) of $TBAPF_6$ was dissolved in 14 mL of 1,1,2-trichloroethane. To one-half of this solution was added 5 mg (0.0142 mmol) of **3a**, and then the suspension was placed in the anodic chamber of the electrocrystallization cell, while the other half containing only the supporting electrolyte was poured in the cathodic compartment. Single crystals of the salt were grown at 20 °C over a period of 14 days on a platinum wire electrode, by applying a constant current of 0.5 μA for 7 days and then of 1 μA for 7 days.

X-ray Structure Determinations. Details about data collection and solution refinement are given in Table 9. X-ray diffraction measurements were performed on a Bruker Kappa CCD diffractometer, operating with a $Mo_{K\alpha}$ (λ = 0.71073 Å) X-ray tube with a graphite monochromator. The structures were solved (SHELXS-97) by direct methods and refined (SHELXL-97) by full matrix least-squares procedures on F^2.[27] All non-hydrogen atoms were refined anisotropically. Hydrogen atoms were introduced at calculated positions (riding model), included in structure factor calculations but not refined. Crystallographic data for the structures have been deposited with the Cambridge Crystallographic Data Centre, deposition numbers CCDC 894781 (**3a**), CCDC 894782 (**3b**), and CCDC 905395 ([(**3a**)(PF_6)]). These data can be obtained free of charge from CCDC, 12 Union road, Cambridge CB2 1EZ, UK (e-mail: deposit@ccdc.cam.ac.uk or http://www.ccdc.cam.ac.uk).

Table 9. Crystallographic Data, Details of Data Collection, and Structure Refinement Parameters

	3a	**3b**	[(**3a**)(PF_6)]
formula	$C_9H_3Cl_2N_3S_4$	$C_{11}H_7Cl_2N_3S_6$	$C_9H_3Cl_2N_3S_4PF_6$
M [g mol^{-1}]	352.28	444.46	497.25
T [K]	293(2)	293(2)	293(2)
crystal system	monoclinic	monoclinic	monoclinic
space group	$P2_1/c$	$P2_1/c$	$P2_1/n$
a [Å]	7.4123(6)	7.0913(5)	9.7138(7)
b [Å]	7.6587(3)	15.9784(15	14.9137(9)
c [Å]	23.2899(16)	15.2724(12)	12.1657(6)
β [deg]	98.775(5)	94.935(7)	112.131(5)
V [Å^3]	1306.66(15)	1724.1(2)	1632.58(17)
Z	4	4	4
ρ_{calcd} [g cm^{-3}]	1.791	1.712	2.023
μ [mm^{-1}]	1.117	1.146	1.070
GOF on F^2	1.031	1.099	1.026
final R1/wR2 [$I > 2\sigma(I)$]	0.0437/0.0736	0.0551/0.1041	0.0670/0.1666
R1/wR2 (all data)	0.0946/0.0861	0.1002/0.1168	0.1100/0.1978

Electrochemical Studies. Cyclic voltammetry measurements were carried out with a Biologic SP-150 potentiostat in a glovebox containing dry, oxygen-free (<1 ppm) argon at 293 K, by using a three-electrode cell equipped with a platinum millielectrode of 0.126 cm^2 area, an Ag/Ag^+ pseudoreference electrode, and a platinum wire counter electrode. The potential values were then readjusted with respect to the saturated calomel electrode (SCE). The electrolytic media involved a 0.1 mol/L solution of (n-Bu_4N)PF_6 in CH_2Cl_2/acetonitrile (1:1) (for **3a** and **3b**) or THF (for **4b**). All experiments were performed at room temperature at 0.1 V/s.

Photophysics. Solvents dichloromethane (DCM), acetonitrile, cyclohexane, toluene, and *N*,*N*-dimethylformamide (DMF), always of the best available quality for photophysics and electrochemistry, were purchased from commercial sources and used as received without further purification. UV−vis absorption spectra were measured on a Cary 5000 spectrophotometer. Steady-state emission spectra were recorded on a Fluorolog 3 spectrophotometer.

For steady-state luminescence measurements, solution samples with proper concentrations were prepared by dilution from the standard solution such that OD at the irradiation wavelength was <0.1. They were deoxygenated by bubbling dry nitrogen for 30 min in a 1 cm path-length quartz cell prior to measurements. Precautions were taken to limit exposure of the photosensitive complexes to light between measurements and during bubbling with nitrogen.

Theoretical Calculations. All calculations have been performed with the Gaussian 09 program package.[26] The geometry optimizations and the TDDFT electronic excitation calculations were carried out with the PBE0 functional.[25]

■ ASSOCIATED CONTENT

Ⓢ Supporting Information

X-ray crystallographic file in CIF format, structural details, UV−vis spectroscopy and photophysics of the neutral and oxidized forms, and theoretical calculations. This material is available free of charge via the Internet at http://pubs.acs.org.

■ AUTHOR INFORMATION

Corresponding Author

*Tel.: (+33)02 41 73 54 92 (N.A.). Fax: (+33)02 41 73 54 05 (N.A.). E-mail: narcis.avarvari@univ-angers.fr (N.A.); andreas.hauser@unige.ch (A.H.).

Notes

The authors declare no competing financial interest.

dx.doi.org/10.1021/ic3027336 | *Inorg. Chem.* 2013, 52, 5023−5034

■ ACKNOWLEDGMENTS

Financial support from the CNRS, the University of Angers, and the National Agency for Research (ANR, Project 09-BLAN-0045-01) as well as the Swiss National Science Foundation (Grant No. 200020-137567) is gratefully acknowledged. C. Mézière is thanked for the MS and elemental analyses.

■ REFERENCES

(1) Brédas, J.-L.; Beljonne, D.; Coropceanu, V.; Cornil, J. *Chem. Rev.* **2004**, *104*, 4971−5004.
(2) (a) Segura, J. L.; Martin, N. *Angew. Chem., Int. Ed.* **2001**, *40*, 1372−1409. (b) Canevet, D.; Sallé, M.; Zhang, G. X.; Zhang, D. Q.; Zhu, D. B. *Chem. Commun.* **2009**, 2245−2269.
(3) Jeppesen, J. O.; Nielsen, M. B.; Becher, J. *Chem. Rev.* **2004**, *104*, 5115−5131.
(4) (a) Bryce, M. R. *Adv. Mater.* **1999**, *11*, 11−23. (b) Bendikov, M.; Wudl, F.; Perepichka, D. F. *Chem. Rev.* **2004**, *104*, 4891−4945.
(5) (a) Jia, C.; Liu, S.-X.; Tanner, C.; Leiggener, C.; Neels, A.; Sanguinet, L.; Levillain, E.; Leutwyler, S.; Hauser, A.; Decurtins, S. *Chem.-Eur. J.* **2007**, *13*, 3804−3812. (b) Dupont, N.; Ran, Y.-F.; Jia, H.-P.; Grilj, J.; Ding, J.; Liu, S.-X.; Decurtins, S.; Hauser, A. *Inorg. Chem.* **2011**, *50*, 3295−3303. (c) El-Khouly, M. E.; Jaggi, M.; Schmid, B.; Blum, C.; Liu, S.-X.; Decurtins, S.; Ohkubo, K.; Fukuzumi, S. *J. Phys. Chem. C* **2011**, *115*, 8325−8334. (d) Otón, F.; Lloveras, V.; Mas-Torrent, M.; Vidal-Gancedo, J.; Veciana, J.; Rovira, C. *Angew. Chem., Int. Ed.* **2011**, *50*, 10902−10906. (e) Jia, H.; Schmid, B.; Liu, S.-X.; Jaggi, M.; Monbaron, P.; Bhosale, S. V.; Rivadehi, S.; Langford, S. J.; Sanguinet, L.; Levillain, E.; El-Khouly, M. E.; Morita, Y.; Fukuzumi, S.; Decurtins, S. *ChemPhysChem* **2012**, *13*, 3370−3382.
(6) Pop, F.; Amacher, A.; Avarvari, N.; Ding, J.; Lawson Daku, L. M.; Hauser, A.; Koch, M.; Hauser, J.; Liu, S.-X.; Decurtins, S. *Chem.-Eur. J.* **2013**, *19*, 2504−2514.
(7) (a) Levi, O. P.-T.; Becker, J. Y.; Ellern, A.; Khodorkovsky, V. *Tetrahedron Lett.* **2001**, *42*, 1571−1573. (b) Zhu, Q.-Y.; Liu, Y.; Lu, W.; Zhang, Y.; Bian, G.-Q.; Niu, G.-Y.; Dai, J. *Inorg. Chem.* **2007**, *46*, 10065−10070.
(8) Nishida, S.; Morita, Y.; Fukui, K.; Sato, K.; Shiomi, D.; Takui, T.; Nakasuji, K. *Angew. Chem., Int. Ed.* **2005**, *44*, 7277−7280.
(9) Riobé, F.; Grosshans, P.; Sidorenkova, H.; Geoffroy, M.; Avarvari, N. *Chem.-Eur. J.* **2009**, *15*, 380−387.
(10) Branzea, D. G.; Fihey, A.; Cauchy, T.; El-Ghayoury, A.; Avarvari, N. *Inorg. Chem.* **2012**, *51*, 8545−8556.
(11) Lorcy, D.; Bellec, N.; Fourmigué, M.; Avarvari, N. *Coord. Chem. Rev.* **2009**, *253*, 1398−1438.
(12) (a) de Hoog, P.; Gamez, P.; Driessen, W. L.; Reedijk, J. *Tetrahedron Lett.* **2002**, *43*, 6783−6786. (b) Steffensen, M. B.; Simanek, E. E. *Angew. Chem., Int. Ed.* **2004**, *43*, 5178−5180. (c) Wang, M.-X.; Yang, H.-B. *J. Am. Chem. Soc.* **2004**, *126*, 15412−15422.
(13) (a) Fink, R.; Frenz, C.; Thelakkat, M.; Schmidt, H.-W. *Macromolecules* **1997**, *30*, 8177−8181. (b) Wang, W.; Sun, H.; Kaifer, A. E. *Org. Lett.* **2007**, *9*, 2657−2660. (c) Chérioux, F.; Maillotte, H.; Audebert, P.; Zyss, J. *Chem. Commun.* **1999**, 2083−2084. (d) Cui, Y.-Z.; Fang, Q.; Xue, G.; Xu, G.-B.; Yin, L.; Yu, W.-T. *Chem. Lett.* **2005**, *34*, 644−648. (e) Pang, J.; Tao, Y.; Freiberg, S.; Yang, X.-P.; D'Iorio, M.; Wang, S. *J. Mater. Chem.* **2002**, *12*, 206−212.
(14) García, A.; Insuasty, B.; Ángeles Herranz, M.; Martin-Álvarez, R.; Martin, N. *Org. Lett.* **2009**, *11*, 5398−5401.
(15) Riobé, F.; Avarvari, N.; Grosshans, P.; Sidorenkova, H.; Berclaz, T.; Geoffroy, M. *Phys. Chem. Chem. Phys.* **2010**, *12*, 9650−9660.
(16) Iyoda, M.; Hara, K.; Kuwatani, Y.; Nagase, S. *Org. Lett.* **2000**, *2*, 2217−2220.
(17) Stueber, G. J.; Kieninger, M.; Schettler, H.; Busch, W.; Goeller, B.; Franke, J.; Kramer, H. E. A.; Hoier, H.; Henkel, S.; Fischer, P.; Port, H.; Hirsch, T.; Rytz, G.; Birbaum, J.-L. *J. Phys. Chem.* **1995**, *99*, 10097−10109.
(18) Goze, C.; Leiggener, C.; Liu, S.-X.; Sanguinet, L.; Levillain, E.; Hauser, A.; Decurtins, S. *ChemPhysChem* **2007**, *8*, 1504−1512.
(19) Ashton, P. R.; Balzani, V.; Becher, J.; Credi, A.; Fyfe, M. C. T.; Mattersteig, G.; Menzer, S.; Nielsen, M. B.; Raymo, F. M.; Stoddart, J. F.; Venturi, M.; Williams, D. J. *J. Am. Chem. Soc.* **1999**, *121*, 3951−3957.
(20) Pou-AméRigo, R.; Ortí, E.; Merchán, M.; Rubio, M.; Viruela, P. M. *J. Phys. Chem. A* **2002**, *106*, 631−640.
(21) (a) Khodorkovsky, V.; Shapiro, L.; Krief, P.; Shames, A.; Mabon, G.; Gorgues, A.; Giffard, M. *Chem. Commun.* **2001**, 2736−2737. (b) Kirketerp, M.-B. S.; Espinosa Leal, L. A.; Varsano, D.; Rubio, A.; Jørgensen, T. J. D.; Kilså, K.; Nielsen, M. B.; Nielsen, S. B. *Chem. Commun.* **2011**, *47*, 6900−6902.
(22) Rosokha, S. V.; Kochi, J. K. *J. Am. Chem. Soc.* **2007**, *129*, 828−838.
(23) Jia, C.; Ding, J.; Liu, S.-X.; Labat, G.; Neels, A.; Hauser, A.; Decurtins, S. *Polyhedron* **2013**, DOI: POLY-D-13-00031.
(24) (a) Hohenberg, P.; Kohn, W. *Phys. Rev.* **1964**, *136*, B864−B871. (b) Kohn, W.; Sham, L. J. *Phys. Rev.* **1965**, *140*, A1133−A1138.
(25) (a) Casida, M. E. In *Recent Advances in Density Functional Methods*; Chong, D. P., Ed.; World Scientific: Singapore, 1995. (b) Burke, K.; Ernzerhof, M.; Perdew, J. P. *Chem. Phys. Lett.* **1997**, *265*, 115−120. (c) Adamo, C.; Barone, V. *J. Chem. Phys.* **1999**, *110*, 6158−6170.
(26) *Gaussian 09*, revision C.01; Gaussian, Inc.: Wallingford, CT, 2010. For a full list of authors, see the Supporting Information.
(27) Sheldrick, G. M. *Programs for the Refinement of Crystal Structures*; University of Göttingen: Göttingen, Germany, 1996.